18th International Conference
ENGINEERING MECHANICS 2012
Svratka, Czech Republic, May 14 – 17, 2012

pp. 1331–1342
Paper #57

STRUCTURE OF FLOW FIELDS DOWNSTREAM OF TWO DIFFERENT SWIRL GENERATORS

D. Štefan[*], P. Rudolf[**], S. Muntean[***], R. F. Susan-Resiga[****]

Abstract: *This paper discusses the comparison of the flow fields downstream of two different swirl generators. Both swirl generators are used to imitate the flow at the exit of the hydraulic turbine runner and study spatio-temporal behaviour of the swirling flow in the draft tube (i.e. outlet diffuser part of the hydraulic turbine), which undergoes breakdown into vortex rope. Unsteady CFD computations are carried out for identical Reynolds number. Resulting velocity and vorticity profiles are correlated with the structure of the vortex rope. Difference in excited pressure pulsations is illustrated on amplitude-frequency spectra of static wall pressure.*

Keywords: ***swirl generator, vortex rope, velocity profile, vorticity, pressure fluctuations.***

1. Introduction

Control of energy distribution and electricity production are in last several years considerably influenced by electricity produced from renewable sources highly depending on changes in weather conditions i.e. solar power plants and wind power plants. Pump storage hydro power plants (PSHPP) are proved to be effective to reduce voltage fluctuations in whole distribution power grid. Control ability of PSHPP is connected with operation of turbine in extended area quite far from the best efficiency point (BEP). Unfortunately, operation of Francis turbine with constant pitch of turbine runner (mainly used for PSHPP) at partial discharge, where flow rate $Q < Q_{BEP}$, is connected with occurrence of high swirling flow at the inlet of the draft tube with formation of so called vortex rope. The vortex rope evolution correlates with the vortex breakdown and leads to the high pressure fluctuation in the draft tube. This draft tube surge propagates pressure pulsations into whole machinery system. Moreover, when the frequency of pressure pulsations generated by the vortex rope rotation corresponds with natural frequency of machine unit, it can lead to restriction of turbine operation.

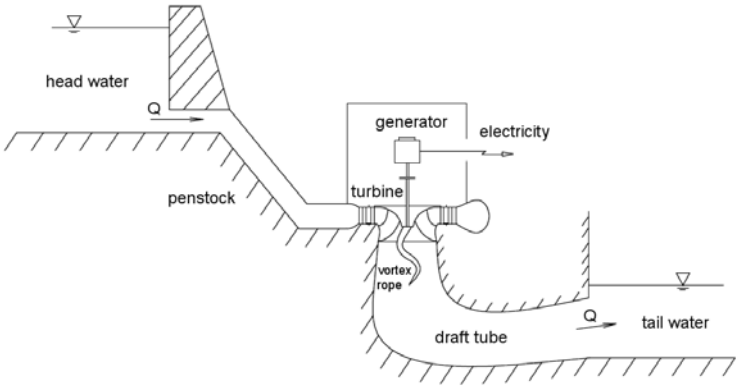

Fig. 1: Cross-sectional schema of hydraulic power plant.

[*] Ing. David Štefan: V. Kaplan Dept. of Fluid Engineering, Faculty of Mechanical Engineering, Brno University of Technology, Technická 2896/2; 61669, Brno; CZ, e-mail: y101274@stud.fme.vutbr.cz

[**] doc. Ing. Pavel Rudolf, Ph.D.: V. Kaplan Dept. of Fluid Engineering, Faculty of Mechanical Engineering, Brno University of Technology, Technická 2896/2; 61669, Brno; CZ, e-mail: rudolf@fme.vutbr.cz

[***] Ing. Sebastian Muntean, Ph.D.: Centre for Advanced Research in Engineering Sciences, Romanian Academy-Timisoara Branch; Bvd. Mihai Viteazu 24; RO-300223, Timisoara; RO, e-mail:seby@acad-tim.tm.edu.ro

[****] prof. Romeo F. Susan-Resiga, Ph.D.: Departmen of Hydraulic Machinery, "Politehnica" University of Timisoara; Bvd. Mihai Viteazu 1; RO-300222, Timisoara; RO, e-mail:resiga@mh.mec.upt.ro

In the last decade, these conclusions lead to large investigation of the swirling flow occurred in the Francis turbine draft tube. As a result, FLINDT (Flow Investigation in Draft Tubes) research project was established with relatively large amount of experimental measured data base describing a wide range of operating points (Avellan 2000, Susan-Resiga 2006). At last time the experimental data base of FLINDT project was employed for various theoretical (Susan-Resiga et al., 2006, Susan-Resiga et al., 2010, Susan-Resiga et al., 2011), experimental (Iliescu et al., 2008) and computational (Ciocan et al., 2007) investigations of swirling flow. Difficulty of the swirling flow investigation in scaled model of hydraulic turbine draft tube leads to idea of building up a simplified apparatus that best imitates flow at the exit of the hydraulic turbine operated at partial discharge.

2. Swirl generators

Swirl generators have been developed at "Politehnica" University of Timisoara as well as at V. Kaplan Dept. of Fluid Engineering, Brno University of Technology. The swirl generators are used to study compactness of generated vortex rope and decay of the vortex rope downstream in the diffuser. Those attributes are farther evaluated with aspect to spectral properties and decrease of the static pressure in vortex rope with respect to the dynamic pressure at the outlet section of swirl generator. Particular design of each referred swirl generator is completely different than the other one.

2.1. Swirl generator RO (SG-RO)

The swirl generator SG-RO has been developed by team at Politehnica University of Timisoara (UPT) and National Center for Engineering Systems with Complex Fluids (NCESCF) as a simplified device to further study the precessing vortex rope (Susan-Resiga et al., 2008a , Petit et al., 2011). The present swirling flow apparatus consists of four leaned strouts, 13 guide vanes, free runner with 10 blades, convergent divergent draft tube (Susan-Resiga et al., 2008a, Bosioc et al., 2008) and is mounted into test rig in hydraulic laboratory at UPT (Bosioc et al., 2009). The stay vanes and runner vanes were designed using inverse design technology in order to create precessing vortex rope (Susan-Resiga et al., 2008b). The swirl flow apparatus is also designed to investigate reduction of the pressure fluctuations of precessing vortex rope by water injection from the nozzle. For this purpose the water supply is provided by auxiliary circuit to leaned strouts.

Design of SG-RO (Susan-Resiga et al., 2008a) is such, that the swirl (i.e. axial and circumferential velocity profiles) in section at the outlet of the runner blades and downstream in convergent divergent section is similar to the Francis turbine investigated in Ciocan et al., 2007.

Numerical simulation of convergent divergent section was carried out by Muntean et al., 2009 and Petit et al., 2011. Both commercial software ANSYS Fluent and open source software OpenFOAM were employed to compute unsteady swirling flow with precessing vortex rope in order to compare the numerical results provided by software codes and experimental results. Due to lower computational requirements the realizable k-ε turbulence model was applied.

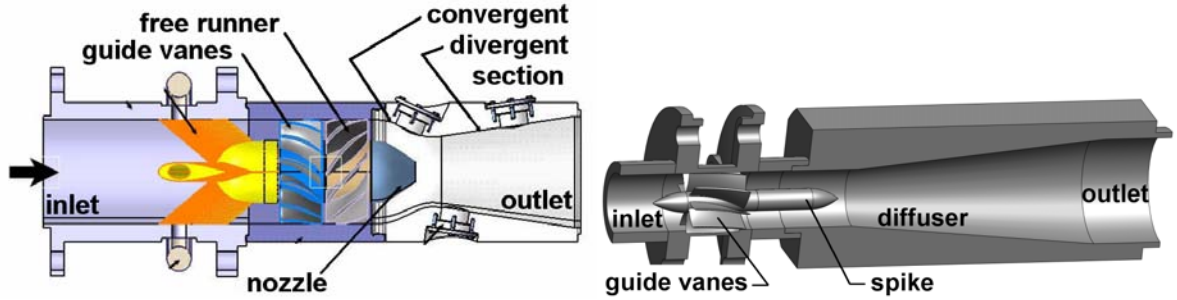

Fig. 2: Experimental setup of swirl generators SG-RO on the left and SG-CZ on the right.

2.2. Swirl generator CZ (SG-CZ)

Differently designed swirl generator has been developed at V. Kaplan Dept. of Fluid Engineering, Faculty of Mechanical Engineering, Brno University of Technology.

The swirl generator consists of 10 fixed blades with relatively long narrow channels to prevent flow separations along the blade surface for a broad range of operating regimes. CFD simulation

proved that almost identical velocity angles are provided by the generator for flow rates between 4 and 13 l/s (Rudolf et al., 2011). The swirl generator is part of test rig placed in hydraulic laboratory of V.K. Dept. of Fluid Engineering. The test rig is supplied from tank by centrifugal pump and swirl generator is situated approximately in the middle of pipeline system. Control of the discharge is enabled via frequency convertor coupled to centrifugal pump.

3. Swirling flow

Swirling flow in diffusers is subject of investigation because of the phenomena (e.g. vortex breakdown, vortex rope), which are not still completely described and understood. Summary of vortex breakdown research can be found in Luca-Negro et al. 2001, where significant influences on vortex rope formation are described.

Experimental and numerical results show, that circumferential velocity profile shape, namely location of the velocity maximum and magnitude of the maximum velocity are decisive for the shape of the cavitating vortical structure (Rudolf et al., 2011). It has to be pointed out, that the two structurally diverse swirl generators produce completely different structure of vortex ropes.

4. CFD calculation

In order to compare swirling flows generated by each swirl generator and resulting vortex rope developing in downstream parts, the unsteady computational study is carried out by commercial software ANSYS Fluent R13 using Reynolds Averaged Navier-Stokes equations (RANS) and Reynolds stress turbulence model (RSM) for turbulence modeling. Considered computational domains are downstream parts of swirl generator apparatuses and diffusers. For better comparison of computed results, we employed RSM turbulence model with higher computational requirements but better performance for highly swirling flow (Jawarneh et al., 2006). The effect of strong turbulence anisotropy can by modeled rigorously only by the second-moment closure adopted in the RSM (Susan-Resiga et al., 2010)

Both computational domains include mesh with approximately 2 million hexahedral cells. The velocity components, turbulence kinetic energy k and dissipation of turbulence kinetic energy ε, obtained from the separate computation of swirl generator part, are defined as the inlet boundary conditions. At the outlet boundary condition is defined constant value of static gauge pressure (0 Pa) with radial equilibrium distribution, where the pressure gradient is governed by the radial component of Euler equation (1).

$$\frac{\partial p}{\partial r} = \frac{\rho v_\theta^2}{r} \tag{1}$$

Where r is distance from the axis of rotation and v_θ is circumferential velocity.

4.1. Computational domain of downstream part of SG-RO

In case of SG-RO the computational domain CD-RO is convergent divergent section with inlet diameter 150 mm, throat diameter D = 100 mm and outlet diameter 160 mm. Survey section S_0 is situated in the throat as a boundary between convergent and divergent section. Survey sections S1, S2 and S3 are in distances 0.5D, D and 1.5D from S_0. Longitudinal cross section of CD-RO with position of survey sections is shown in fig. 3.

4.2. Computational domain of downstream part of SG-CZ

Computational domain CD-CZ as a downstream part of SG-CZ is a diffuser with inlet diameter 53.6 mm, outlet diameter 98 mm and opening angle 12°. Survey section S_0 is placed at the end of cylindrical part with same diameter as the inlet diameter D =53.6 mm. Survey sections S1, S2 and S3 are in distances 0.5D, D and 1.5D from S_0. Longitudinal cross section of CD-RO with position of survey sections is shown in fig. 4.

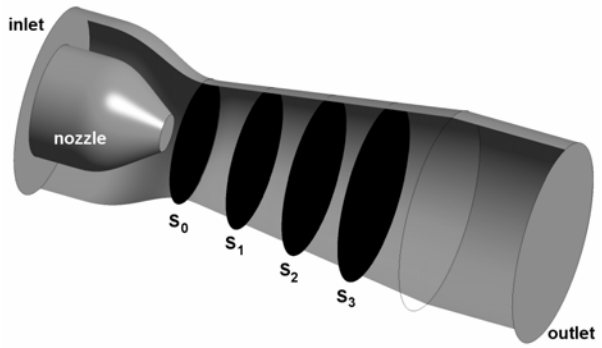

Fig. 3: Computational domain (CD-RO) in case of SG-RO.

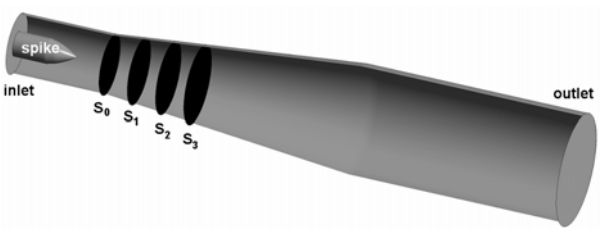

Fig. 4: Computational domain (CD-CZ) in case of SG-CZ.

4.3. Computational set-up

The numerical computations were carried out for flow regimes with identical Reynolds number (2) defined in survey section S_0. The value of Reynolds number is Re = 380143 and corresponds with flow rate Q = 30 l/s for SG-RO and Q = 15.9 l/s for SG-CZ.

$$Re = \frac{\bar{v} \cdot D}{\nu} \tag{2}$$

In fig. 5 are shown velocity profiles generated by SG-RO and in fig. 6 profiles generated by SG-CZ. Those profiles were used as the inlet boundary conditions for numerical computations. Only axial and circumferential components are shown because of very small magnitude of radial velocity component. But in the boundary condition the radial component is included. Velocity components are circumferentially averaged and made dimensionless with respect to the bulk velocity at the outlet of the swirl generator.

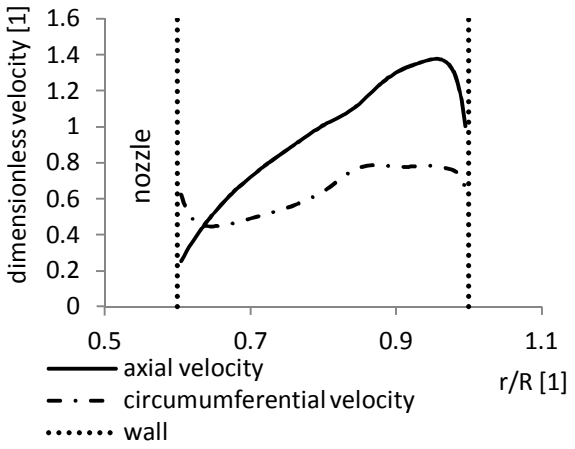

Fig. 5: Velocity components generated by SG-RO.

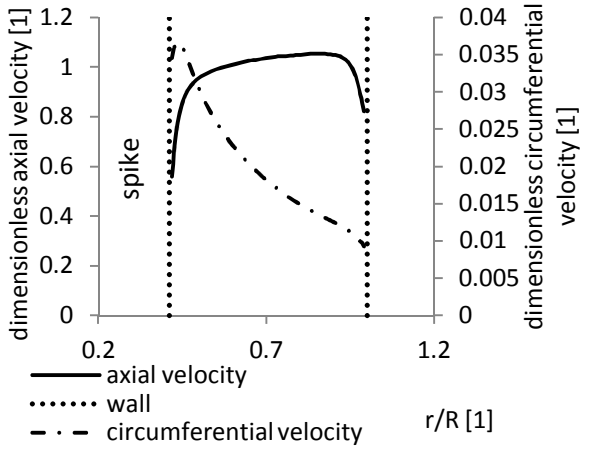

Fig. 6: Velocity components generated by SG-CZ.

5. Evaluation and results

For global quantitative description of the swirling flow we used swirl number (3) defined as the axial flux of swirl momentum divided by the axial flux of axial momentum (Susan-Resiga et al., 2006, Susan-Resiga et al., 2009)

$$S_n = \frac{\int v_{ax} v_{tan} r dS}{R \int v_{ax}^2 dS} \tag{3}$$

Computed value of swirl number generated by SG-RO is $S_{n\text{-}RO}$ = 0,581 and is substantially larger than swirl number computed in case of SG-CZ where $S_{n\text{-}CZ}$ = 0,122. This difference is also noticeable in dimensionless circumferential velocity components, see fig. 5 and fig. 6. Comparison for identical swirl number is not carried out due to different design of swirl generators (blade design of SG- CZ produces much smaller circumferential velocity component than SG-RO).

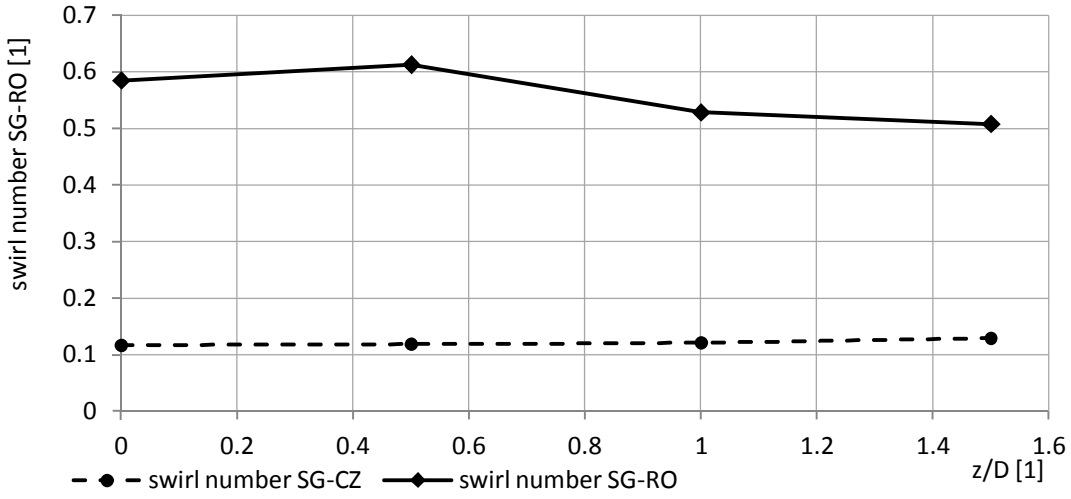

Fig. 7: Swirl number streamwise development in case of CD-RO (solid line) and CD-CZ (dashed line).

5.1. Velocity profiles computed in survey section S_0

Velocity profiles computed in survey sections S_0 are time averaged and made dimensionless with respect to equation (4).

$$v_{dim-less} = \frac{v}{\frac{Q}{S}} = \frac{v}{\bar{v}} \tag{4}$$

Where v is corresponding velocity component and $\bar{v}$ is bulk velocity defined as a flow rate Q divided by cross-sectional area S.

In figure are plotted dimensionless axial velocity components and in fig. 9 circumferential velocity components computed in survey section of the corresponding swirl generator.

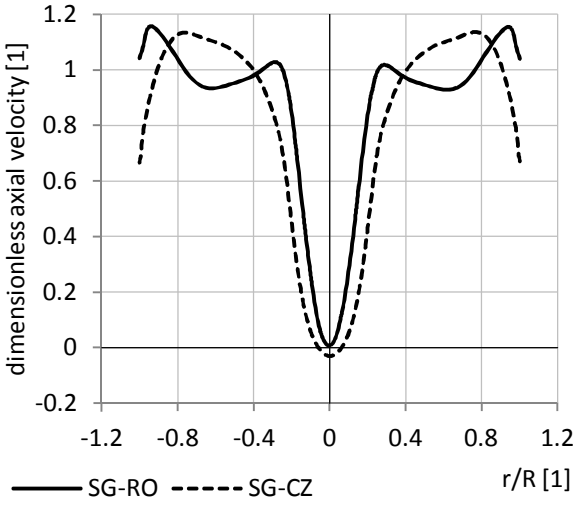

Fig. 8: Dimensionless axial velocity components computed in survey section S0.

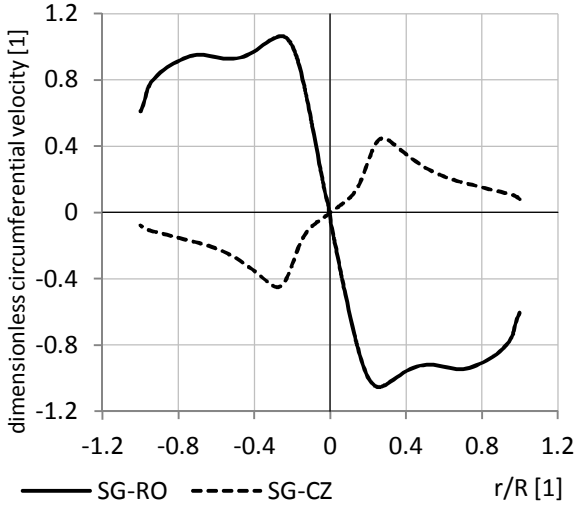

Fig. 9: Dimensionless circumferential velocity components computed in survey section S0.

5.2. Streamwise evolution of axial velocity, circumferential velocity and vorticity magnitude

Evolution of axial velocity components along the diffuser axis are shown in figs. 10 and 13. Enlargement of stagnant region is evident and related with extending of vortex rope helix in streamwise direction. Axial velocity component is much larger in case of SG-CZ than in case of SG-RO. On the other hand circumferential velocity component is much smaller in case of SG-CZ than in case of SG-RO. Different sense of flow rotation, caused by different design of swirl generators, is noticeable in circumferential velocity profiles (see fig. 11 versus fig. 14 or fig. 9). Magnitudes of corresponding profiles (axial, circumferential or vorticity) are plotted in equal dimensional scale.

Important fact is, that boundary of stagnant region (apparent by the large gradient of velocity profile curve), is in appropriate distance from the diffuser axis for both, axial and circumferential velocity component. This fact shows strong coupling between corresponding axial and circumferential velocities (Batchelor, 1964).

Vorticity magnitude profiles evolution (fig. 12 versus fig. 15) shows higher compactness of vortex core in streamwise direction (significant peaks of vorticity) for case of SG-CZ. This conclusion is evident in fig. 18, where streamlines in combination with vortex core are shown. Abrupt vortex decay, approximately situated near survey section S1, is apparent in case of SG-RO. This abrupt vortex decay is also probably related with formation of huge backflow region (visualized in fig. 17 (left) as a time averaged) and linked with significant longitudinal vortex rope pulsation with computed frequency around 2.5Hz (see figs. 23 and 24).

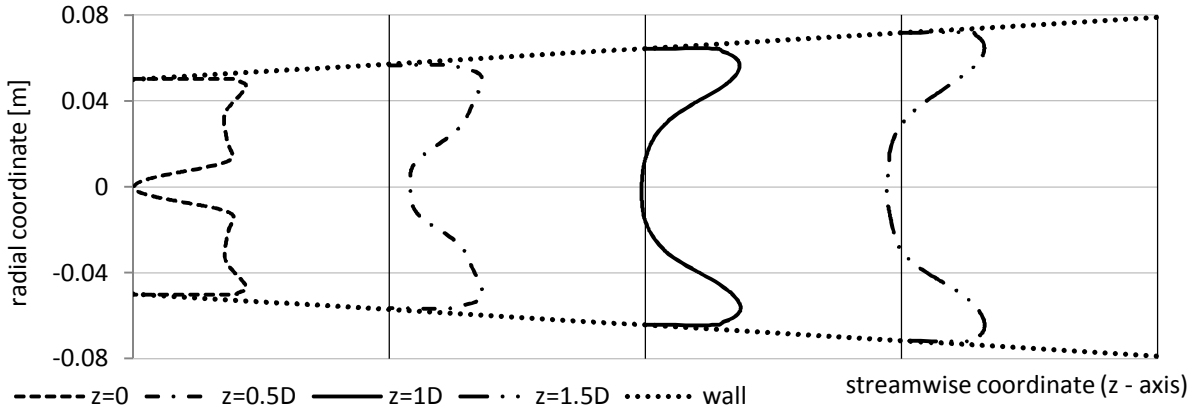

Fig. 10: Time averaged axial velocity profile development downstream in diffuser of CD-RO.

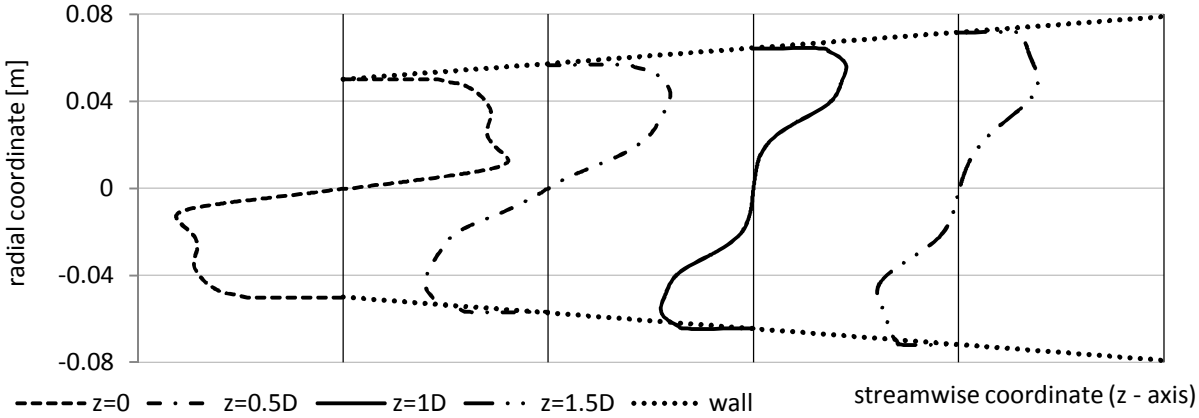

Fig. 11: Time averaged circumferential velocity profile development downstream in diffuser of CD-RO.

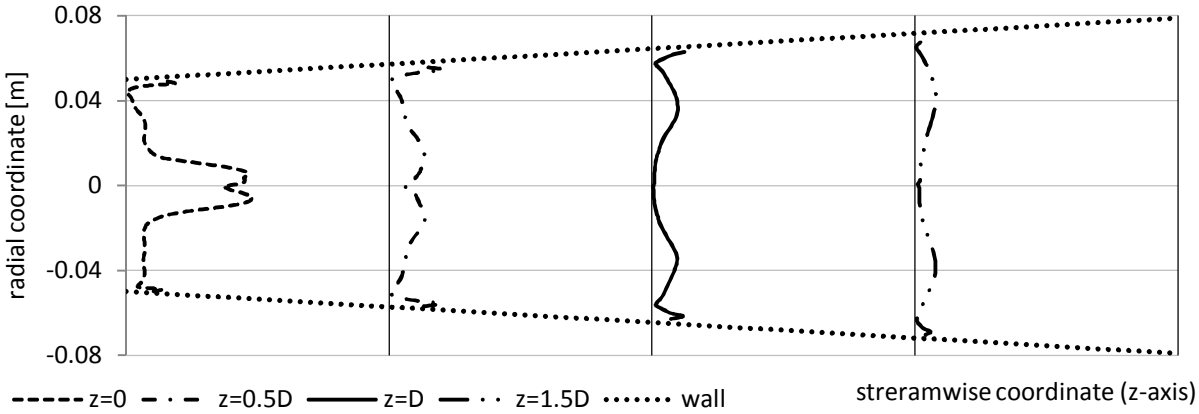

Fig. 12: Time averaged vorticity magnitude profile development downstream in diffuser of CD-RO.

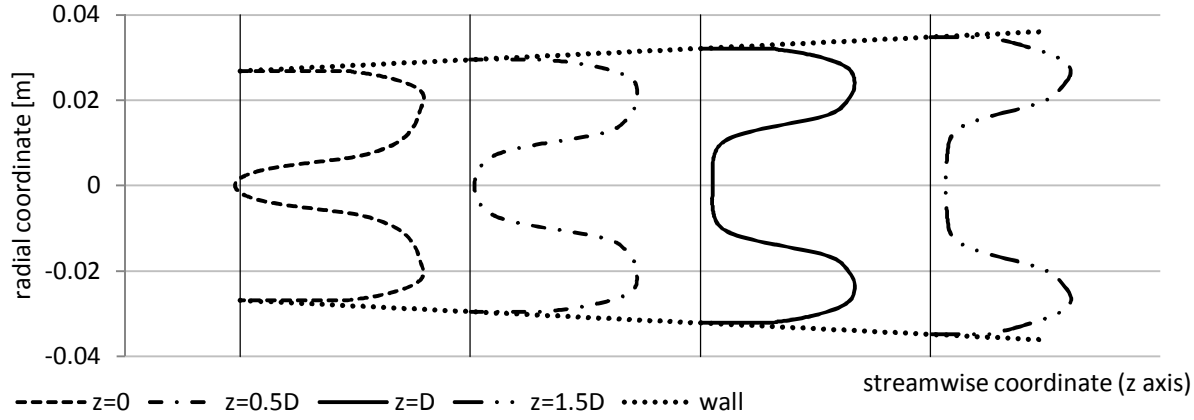

Fig. 13: Time averaged axial velocity profile development downstream in diffuser of CD-CZ.

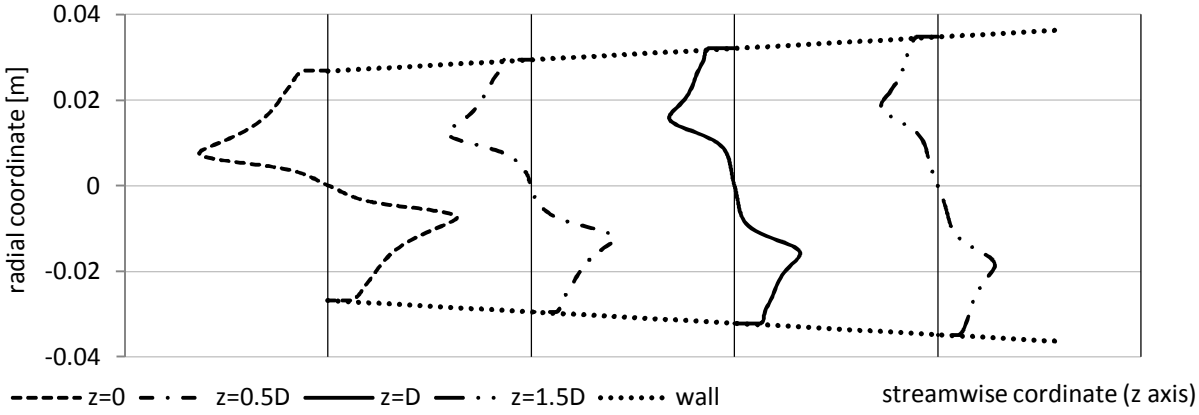

Fig. 14: Time averaged circumferential velocity profile development downstream in diffuser of CD-CZ.

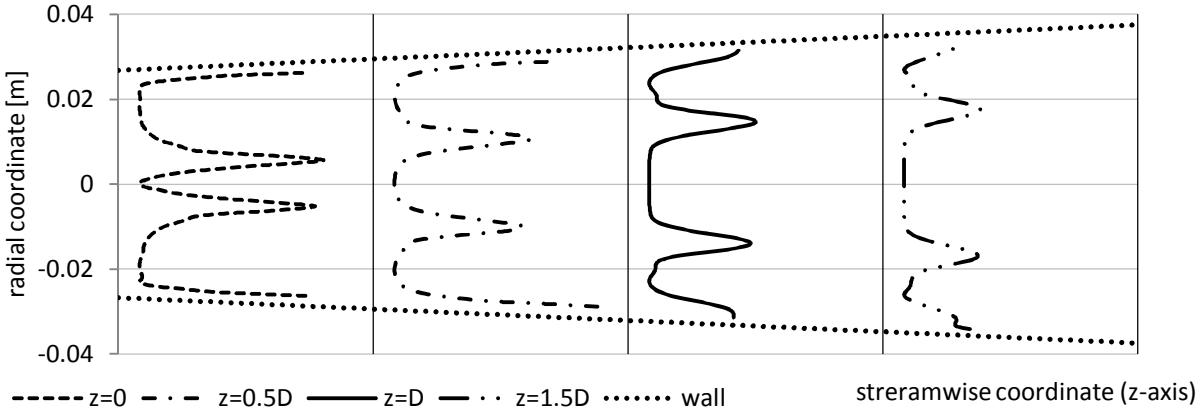

Fig. 15: Time averaged vorticity magnitude profile development downstream in diffuser of CD-CZ.

5.3. Flow field analysis

Calculation is based on one phase model, thus for the vortex rope visualization is applied isosurface of very low pressure. Significant difference between pressure drop generated by each swirl generator is noticeable. Vortex ropes are visualized for ratio p_{stat}/p_{dyn_inlet} = -1.95 in case of SG-RO and -1.08 in case of SG-CZ, where p_{stat} is value of static pressure isosurface and p_{dyn_inlet} is dynamic pressure at the inlet of computational domain. Time snapshot of vortex ropes with corresponding backflow regions are shown in fig. 16. On the other hand time averaged backflow regions are visualized in fig. 17. In fig. 19 is shown longitudinal development of SG-RO vortex rope in time. Time period is around 0.4 s and corresponds with frequency around 2.5 Hz extracted from pressure signal evaluated in section 5.4. Noticeable is transition from one long vortex rope (t = 0s) to one longer and one very short intertwined vortex ropes (t = 0.1s or 0.2s).

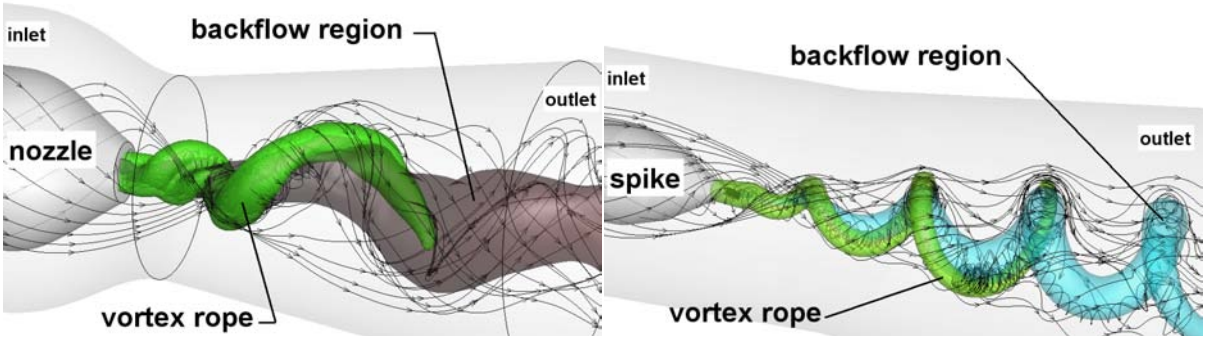

Fig. 16: Vortex rope and instantaneous snapshot of backflow region, CD-RO on the left and CD-CZ on the right.

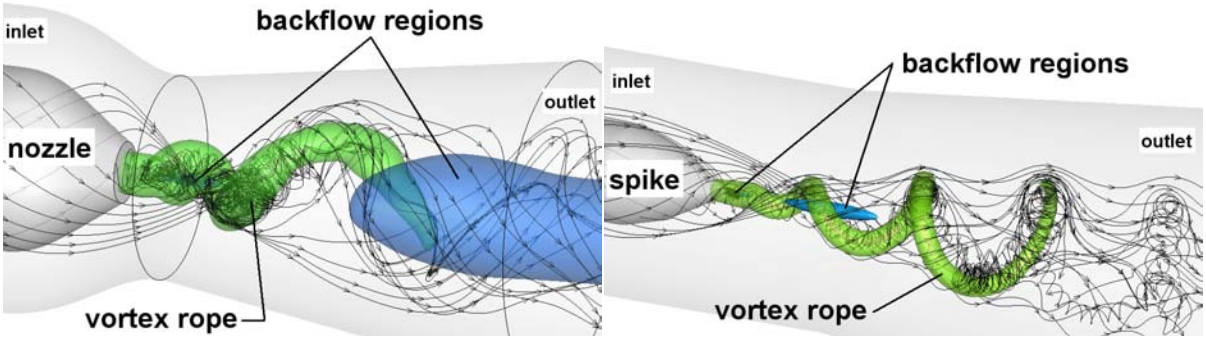

Fig. 17: Vortex rope and time averaged backflow regions, CD-RO on the left and CD-CZ on the right.

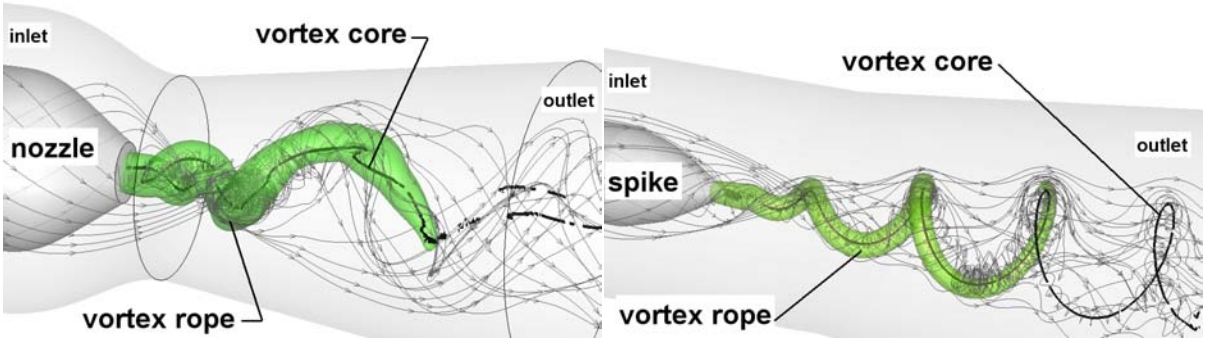

Fig. 18: Vortex rope and vortex core region, CD-RO on the left and CD-CZ on the right.

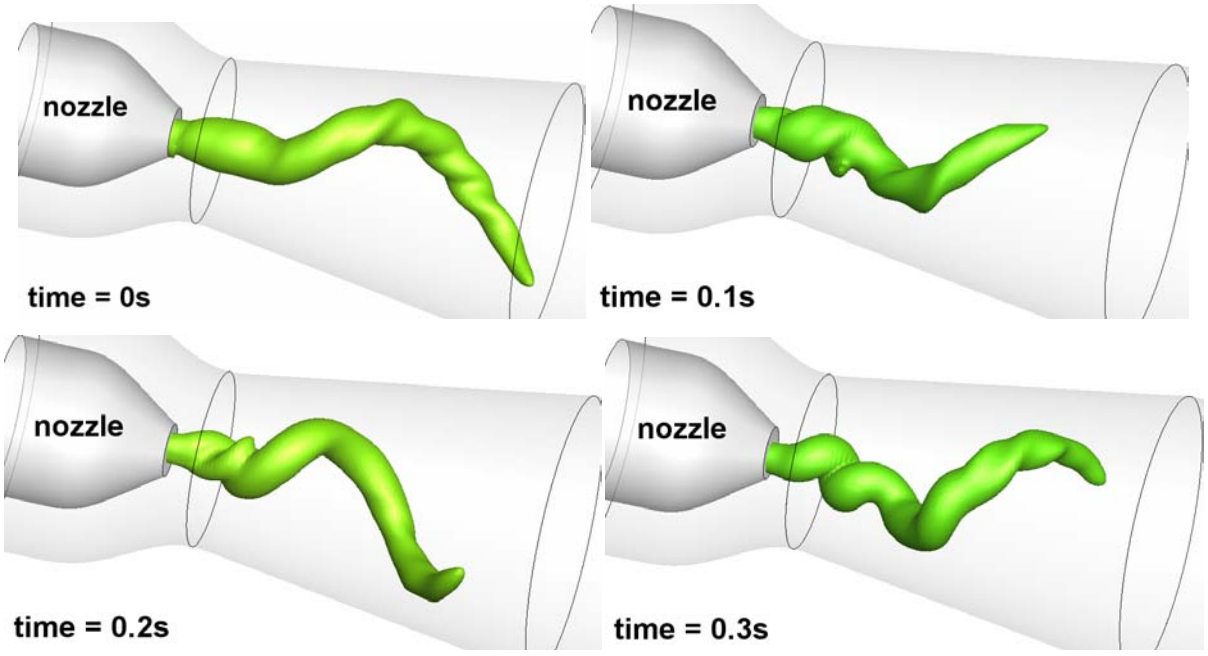

Fig. 19: Longitudinal development of SG-RO vortex rope in time

5.3.1. Comparison with experimental measurement

In this section axial and circumferential velocity components extracted from CFD computation are compared with experimentally measured velocity components carried out by 2D LDV measurement in case of SG-RO (Bosioc et al., 2009), see fig. 20. Comparison is carried out for two survey sections corresponding with window W1 (plotted in fig. 21) and window W2 (plotted in fig. 22). One can see good fitting of numerical curves with experimentally measured axial velocity. Higher discrepancy appears in circumferential velocity component outside of the diffuser axis. Computed circumferential velocity profiles are flatter than the measured ones.

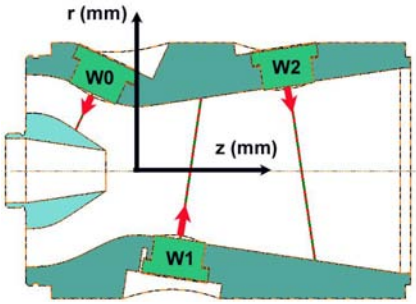

Fig. 20: Survey axis for LDV measurement in convergent divergent part of SG-RO (Bosioc et al., 2009).

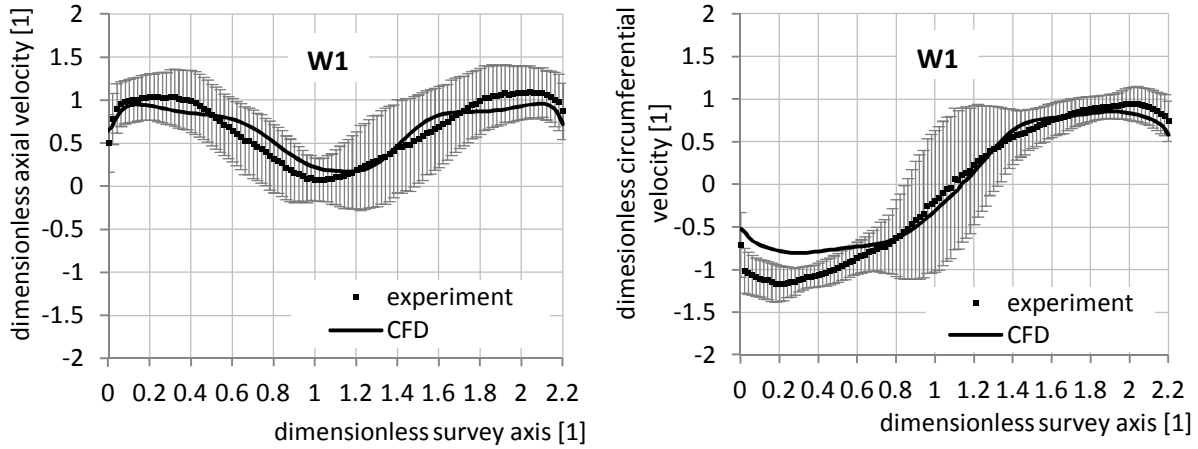

Fig. 21: Velocity components from 2D LDV measurement compared with CFD results (window W1).

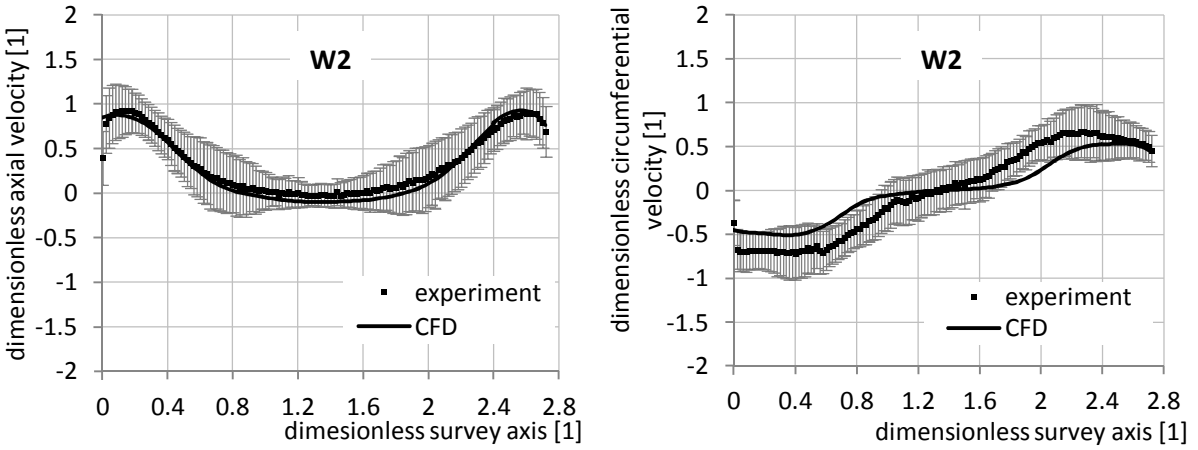

Fig. 22: Velocity components from 2D LDV measurement compared with CFD results (window W2).

5.4. Fourier analysis of the pressure fluctuations

As a results of vortex breakdown high pressure fluctuations are generated in downstream part of swirl generator. Time record of numerically computed static pressure was set in four monitoring points to perform Fast Fourier Analysis. The monitoring points are situated near the wall of the computational domain in downstream distances in order 0, 0.5D, D and 1.5D from S_0, where D is diameter of survey

section S_0. Simply script written in MATLAB software was employed to extract spectral information of the numerical pressure record. Frequencies with dominant amplitude are shown in tab. 1 for CD-RO and in tab. 2 for CD-CZ. In fourth column are amplitudes related to the inlet dynamic pressure p_{dyn}.

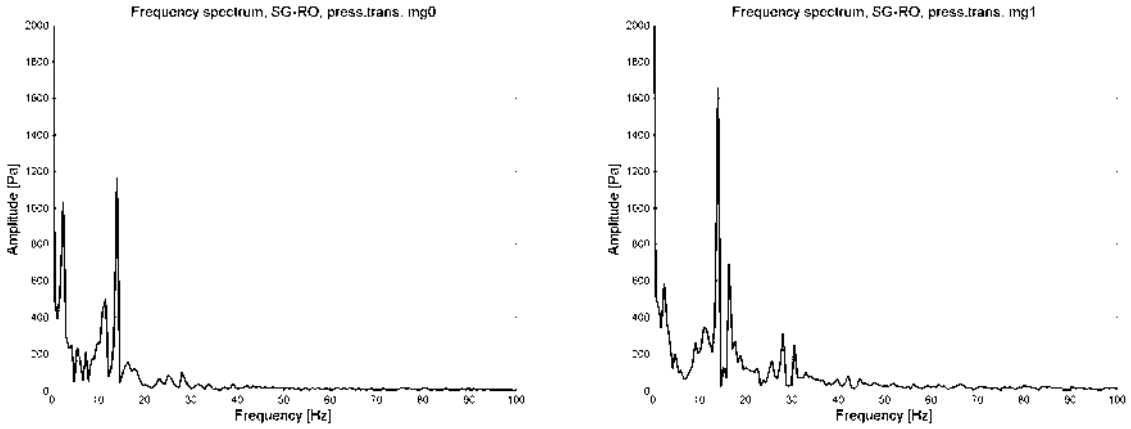

Fig. 23: Amplitude-frequency spectrum of pressure pulsations in case of CD-RO (MG0 on the left, MG1 on the right).

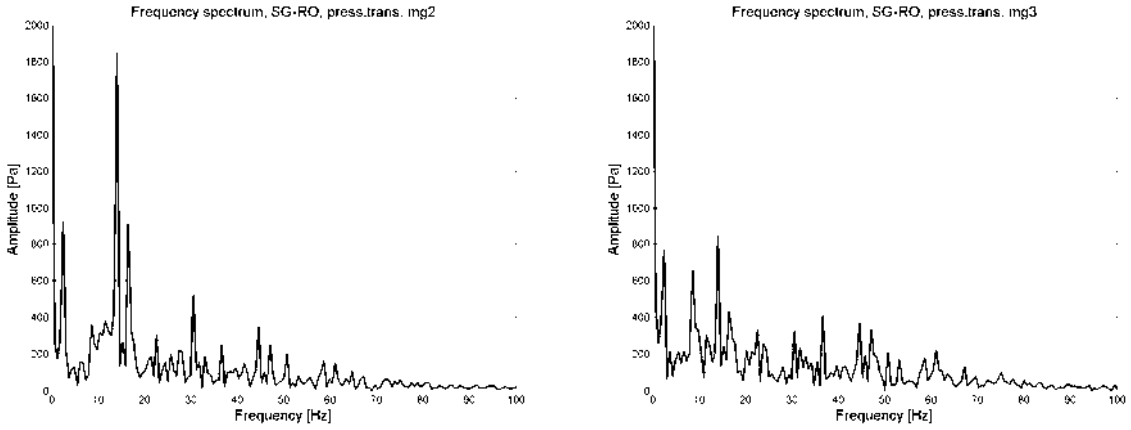

Fig. 24: Amplitude-frequency spectrum of pressure pulsations in case of CD-RO (MG2 on the left, MG3 on the right).

Tab. 1: Spectral analysis of CD- RO

Monitoring point	Dominant frequency [Hz]	Amplitude [Pa]	Amplitude/p_{dyn} [1]
MG0	14.04	1166	0.189
MG1	14.04	1655	0.268
MG2	14.04	1847	0.299
MG3	14.04	843	0.137

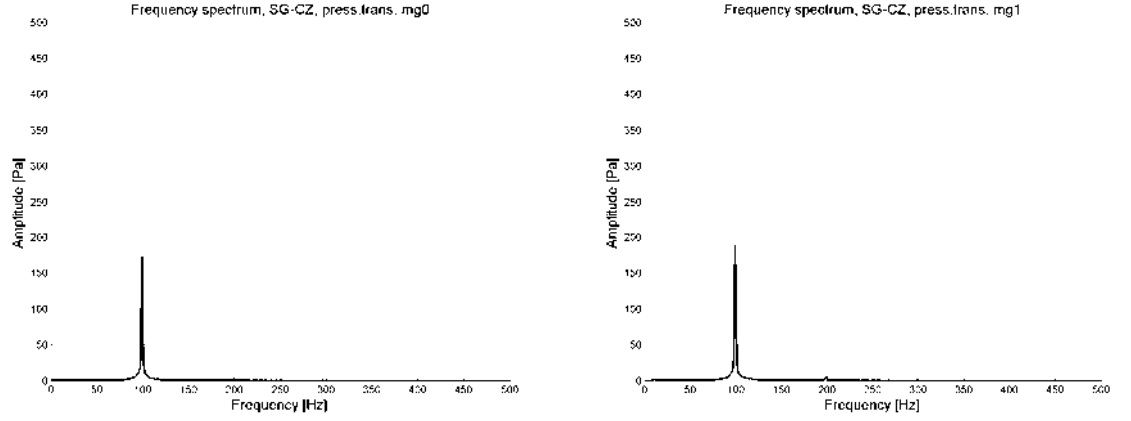

Fig. 25: Amplitude-frequency spectrum of pressure pulsations in case of CD-CZ (MG0 on the left, MG1 on the right).

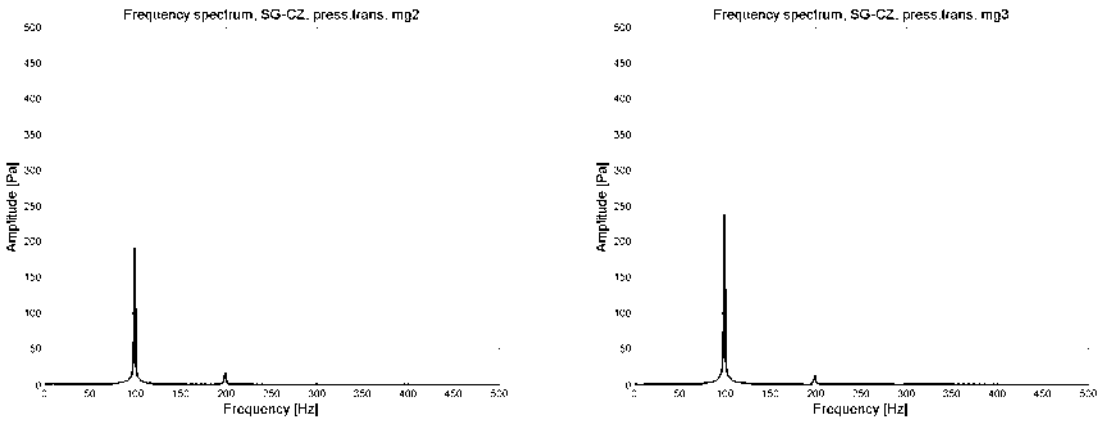

Fig. 26 Amplitude-frequency spectrum of pressure pulsations in case of CD-RO (MG2 on the left, MG3 on the right).

Tab. 2: Spectral analysis of CD- CZ

Monitoring point	Dominant frequency [Hz]	Amplitude [Pa]	Amplitude/p_{dyn} [1]
MG0	99.46	172.5	$3.37 \cdot 10^{-3}$
MG1	99.46	189.9	$5.02 \cdot 10^{-3}$
MG2	99.46	191	$5.04 \cdot 10^{-3}$
MG3	99.46	237.4	$6.28 \cdot 10^{-3}$

5.4.1. Comparison with experimental measurement

Experimentally measured frequency of vortex rope rotation in case of SG-RO is found around 14.95Hz. One can see only small difference (6%) between experimentally measured and numerically computed frequency and good agreement with previous computational results (Muntean et al., 2009, Petit et al., 2011). Lower value of numerical frequency confirms that numerical model is more dissipative than experiment. Suitable agreement in comparison of numerical and experimental (Muntean et al., 2009) amplitude magnitude is obtained only for pressure transducers MG0, while computed amplitudes for MG1, MG2 and MG3 overestimate experimental results. Comparison for case of SG-CZ is not carried out because of high interference in experimental data. This problem is being further investigated.

6. Conclusions

Different shape of vortex rope, generated by each swirl generator, corresponds with different value of swirl number. SG-RO with higher swirl number than SG-CZ composes swirling flow with more massive vortex rope. Vortex rope has larger width and forms into shape with higher ascend of helix. This shape is similar to the vortex rope appearing in Francis turbine draft tube (FLINDT project) during operation on 70% Q_{BEP} and was main designed parameter of SG-RO.

On the other hand, vortex rope generated by SG-CZ is thinner and forms into shape with lower ascend of the helix. In comparison with the vortex ropes computed in paper Rudolf 2009 for inlet boundary conditions derived by Susan-Resiga et al., 2006, the vortex rope generated by SG-CZ is very similar one to the vortex rope corresponding with the turbine operation on 90%Q_{BEP}.

During calculation it has been observed, that shape of vortex rope generated by SG-RO is in time more unstable than vortex rope generated by SG-CZ. Moreover for calculation with employing of RSM turbulence, the vortex rope changes its structure periodically from one long compact vortex rope into two (long and one very short) vortex ropes which are intertwined close to the nozzle. This change is realized in longitudinal direction with frequency around 2.5Hz and amplitudes around 800Pa.

Results confirmed strong coupling between circumferential and axial velocity components and this coupling is full maintained in streamwise direction.

Acknowledgement

Czech Science Foundation is gratefully acknowledged for support of the research under project No. 101/09/1715 "Cavitating vortical structures induced by rotating liquid". This project is supported by junior research grant number FSI-J-12-21/1698 provided by Brno University of Technology. The Timisoara swirl generator test case and associated experimental data was supported by the Romanian Agency CNCSIS – UEFISCSU, Exploratory Research Project PN II - IDEI 799/2008.

References

Avellan, F. (2000) Flow Investigation in a Francis Draft Tube: The FLINDT Project, in: *Proceedings of the 20th IAHR Symposium on Hydraulic Machinery and Systems*, Charlotte, USA, Paper DES-11.

Batchelor, G. K., (1964) Axial Flow in Trailing Line Vortices, *J. Fluid Mech*., 20 (4), pp. 645–658.

Bosioc, A., Susan-Resiga, R. F., and Muntean, S. (2008) Design and Manufacturing of a Convergent-Divergent Test Section for Swirling Flow Apparatus, in: *Proceedings of the 4th German – Romanian Workshop on Turbomachinery Hydrodynamics* (GRoWTH), June 12-15, 2008, Stuttgart, Germany.

Bosioc, A., Tanasa, C., Muntean, S., Susan-Resiga, R.F. (2009) 2D LDV Measurements of Swirling Flow in a Simplified Draft Tube, in: Proceedings of the CMFF09, Vol. II, Budapest, Hungary. p.p. 833-838

Ciocan, G. D., Iliescu, M. S., Vu, T. C., Nennemann, B., Avellan, F. (2007) Experimental study and numerical simulation of the FLINDT draft tube rotating vortex, *Journal of Fluids Engineering*, Vol. 129, pp.146–158.

Hydrodynamics, Stuttgart, Germany, June 12-15.

Iliescu, M. S., Ciocan, G. D., Avellan, F. (2008) Analysis of the Cavitating Draft Tube Vortex in a Francis Turbine Using Particle Image Velocimetry Measurements in Two-Phase Flow. *Journal of Fluid Engineering.* Vol. 130.

Jawarneh, A. M., Vatistas, G. H. (2006) Reynolds Stress Model in the Prediction of Confined Turbulent Swirling Flows, in: *ASME Journal of Fluid Engineering,* Vol. 128, p.p.1377-1382.

Lucca-Negro, O., O'Doherty, T. (2001) Vortex breakdown: a review, in: Annual Review of Fluid Mechanics, 10, 221-246, 1978.

Muntean, S., Nilsson, H., and Susan-Resiga, R. (2009) 3D Numerical Analysis of the Unsteady Turbulent Swirling Flow in a Conical Diffuser Using Fluent and OpenFOAM, in: *Proceedings of the 3rd IAHR International Meeting of the Workgroup on Cavitation and Dynamic Problem in Hydraulic Machinery and Systems*, Brno, Czech Republic.

Petit, O., Bosioc, A. I., Nilsson, H., Muntean, S., Susan-Resiga, R. F. (2011) Unsteady Simulations of the Flow in a Swirl Generator, Using OpenFOAM, *International Journal of Fluid Machinery and Sytsems,* Vol. 4, No. 1.

Rudolf, P. (2009) Connection between inlet velocity field and diffuser flow instability, in: *Applied and Computational Mechanics,* Vol. 3, No. 1, pp. 177 - 184

Rudolf, P., Hudec, M., Zubík, P., Štefan, D. (2011) Experimental measurement and numerical modeling of cavitating flow in converging-diverging nozzle, in: *Proceedings of the International Conference Experimental Fluid Mechanics 2011*, pp.423-431, Jíčín, Czech Republic.

Susan-Resiga, R. F., Ciocan, G. D., Anton, I., Avellan, F. (2006) Analysis of the swirling flow downstream of a Francis turbine runner. *Journal of Fluid Engineering,* Vol. 128, pp.177-189.

Susan-Resiga, R. F., Muntean, S., and Bosioc, A. (2008b) Blade Design for Swirling Flow Generator, in: *Proceedings of the 4th German – Romanian Workshop on Turbomachinery Hydrodynamics* (GRoWTH), June 12-15, Stuttgart, Germany.

Susan-Resiga, R. F., Muntean, S., Avellan, F., Anton, I. (2011) Mathematical modelling of swirling flow in hydraulic turbines for the full operating range, *Appl. Math. Modell.* doi:10.1016/j.apm.2011.03.052

Susan-Resiga, R. F., Muntean, S., Hasmatuchi, V., Anton, I., Avellan, F. (2010) Analysis and prevention of vortex breakdown in the simplified discharge cone of a Francis turbine, *Journal of Fluid Engineering*, Vol. 132, 15 pages.

Susan-Resiga, R. F., Muntean, S., Stein, P., Avellan, F. (2009) Axisymmetric swirling flow simulation of the draft tube vortex in Francis turbines at partial discharge, in: *Int. J. Fluid Mach. Sys.* 2, pp.295–302.

Susan-Resiga, R. F., Muntean, S., Tanasa, C., Bosioc, A. (2008a) Hydrodynamic Design and Analysis of a Swirling Flow Generator, in: *Proceedings of the 4th German – Romanian Workshop on Turbomachinery Hydrodynamics* (GRoWTH), June 12-15, 2008, Stuttgart, Germany.